Local disorder effects on electron transport in silicon nanostructures

H. Mizuta[1,3], Y. Furuta[1,3], G. Evans[2], K. Nakazato[1,3], T. Kamiya[2,3], Y. T. Tan[2,3], Z. A. K. Durrani[2,3] and H. Ahmed[2,3]

[1] Hitachi Cambridge Laboratory, Hitachi Europe Ltd., Madingley Road, Cambridge, CB3 0HE, UK

[2] Microelectronics Research Centre, University of Cambridge, Madingley Road, Cambridge CB3 0HE, UK

[3] CREST, JST (Japan Science and Technology)

Heavily doped polycrystalline-silicon (poly-Si) and crystalline silicon nanowires (NWs) have widely been used as a building block for Coulomb blockade (CB) memory and logic devices by utilising nanometer-scale electron islands naturally formed by local disorders in the NWs. However, the microscopic properties of the electron islands and tunnel junctions have not been studied in detail, and there has been no clear guideline to optimise the NW materials and structures in terms of high temperature CB device operation. The aim of this work is to clarify and control the local disorder effects on electron transport in the silicon NWs.

In the poly-Si NWs, individual silicon grains and grain boundaries (GBs) act as an electron island and a tunnel junction. In this work we have used heavily doped poly-Si point contact transistors (PC-Trs) where both length and width of the channel are as small as the grain size (see Fig. 1) to investigate electron transport through a single or few GBs. A 50 nm-thick heavily phosphorus-doped (10^{20} cm^{-3}) poly-Si film was formed by solid-phase crystallisation of an amorphous silicon film at 850℃ for 30 min in an Ar ambient. Half the number of PC-Trs were then oxidised at 1000℃ for 15 minutes. An SEM image of the Secco etched poly-Si film (Fig. 1(a)) before exidation shows that the grain size ranges from 20 nm to 150 nm. We have designed the channel length and width of our PC-Trs to be from 30 to 50 nm so that the devices may contain either no GB or a few GBs at most (see Fig. 2). The PC-Trs without oxidation showed linear I_{ds}-V_{ds} characteristics for about 66% of the fabricated devices (Type A) while the rest of the devices (Type B) exhibited non-linear characteristics. The non-linear characteristics for Type B are attributed to the potential barriers of the GBs in the ultra short channel region. From the temperature dependence of resistivity the effective potential barrier height qV_B of the GBs was found to be from 30 meV to 80 meV (see Fig. 3). In contrast with these PC-Trs without oxidation clear CB oscillations have been observed for the oxidised PC-Trs: two typical oscillations are shown in Fig. 4(a) (Oxidised A) and Fig. 4(b) (Oxidised B). Oxidised A has much lower Coulomb gap and a shorter oscillation period than those for Oxidised B, and it is apparent that size of the grain responsible for the CB oscillation of Oxidised B is much smaller than that of Oxidised A. Figures 4(a) and (b) also shows that the ON/OFF ratio of Oxidised B is much larger than that for Oxidised A. We extracted qV_B and tunnel resistance R_T and found that both quantities were larger for Oxidised B (qV_B = 87.6 meV and R_T = 1.01×10^6 Ω) than for Oxidised A (qV_B = 36.4 meV and R_T = 2.89×10^5 Ω). In the oxidation process GBs are converted to sub-oxide SiO_x with $x \ll 2$ since the oxidation at high temperature is limited by oxygen atoms diffused through GBs from device surfaces. The fluctuation of the tunnel barrier parameters indicates that both the band-offset and thickness of SiO_x vary locally. In the present devices, the CB oscillations were washed out at T > 40K, but optimisation of the oxidation process is currently investigated to improve the operating temperature.

In the crystalline silicon NWs, local potential disorder caused by random ionized dopants is responsible for forming the electron islands. For investigating this effect, we have performed a numerical simulation of the silicon NWs, in which random dopant distribution is explicitly treated and the electron distribution is calculated self-consistently. Figure 5 shows an example of a 2D bare dopant potential landscape in the absence of electrons calculated for a 400-nm-long rectangular parallelepiped NW with a cross sectional area of 20 nm x 10 nm with donor concentration of 10^{19} cm^{-3}. A typical sample result from the final electron distribution calculation is shown in Fig. 6. The near-continuous case (Fig. 6(a)) breaks up into islands that merge and disappear as the wire becomes successively more depleted. It should be noted that the electron distribution in the NW is described as a quasi-linear chain of multiple islands. To investigate the offset charge effects on the threshold voltage V_{th}, we calculated the capacitance and tunnel resistance between all the islands and then fed them into the Monte Carlo single-electron transport simulator. The V_{th} distribution obtained for the NW structure shown in Fig. 6(e) is shown in Fig. 7. An analytical model of V_{th} predicts that the distribution is a piece-wise continuous polynomial of maximum degree N −1, where N is the number of islands in the NW. For the case of Fig. 6(e) with N = 7, however, the distribution can be approximated by a piece-wise linear function, for which N = 2. This suggests that the seven islands are grouped into two sets, i.e. the three on the left and the four on the right, with tunnel resistances between these ‘macro’ islands at least an order of magnitude larger than those within the macro-islands (see bottom figure in Fig. 7).

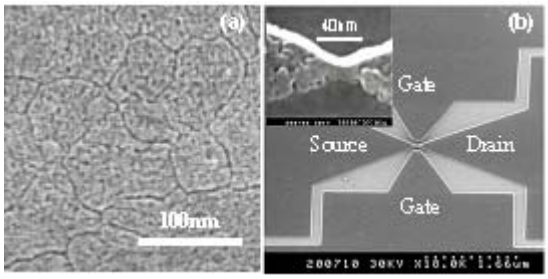

Fig. 1. (a) An scanning electron microscope (SEM) image of a poly-Si film after Secco etching. (b) An SEM image of a point contact transistor (PC-Tr) with a blow-up of the channel (the inset).

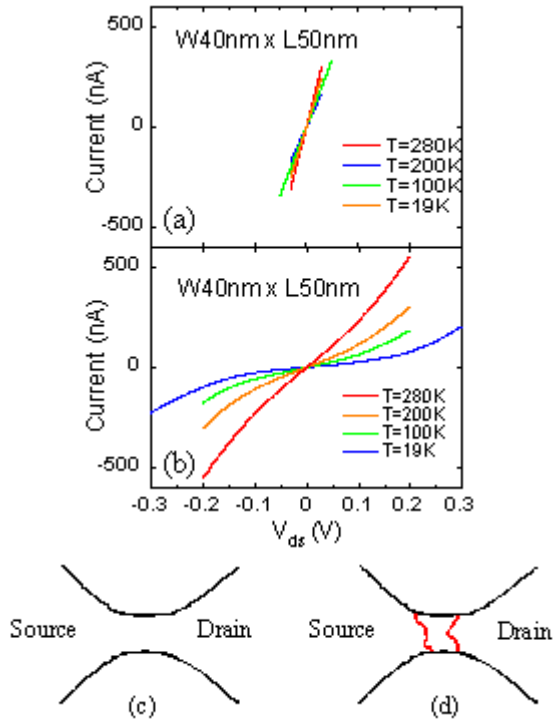

Fig. 2 Ids-Vds characteristics observed for (a) Type A and (b) Type B with a width a width of 40 nm and a length of 50 nm at temperatures ranging from 19K to 280K. A schematic drawing of PC-Trs (c) without and (d) with GBs in the channel, corresponding to Type A and Type B, respectively.

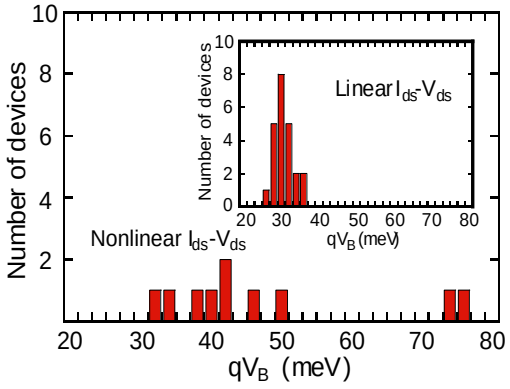

Fig.3 Distribution of potential barrier height qV_B for Type B with nonlinear I_{ds}-V_{ds} characteristics. The inset shows that for Type A with linear I_{ds}-V_{ds} characteristics.

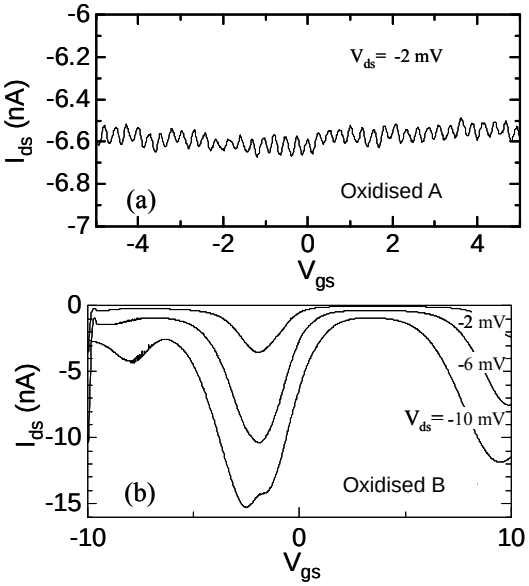

Fig. 4. Two types of Coulomb-blockade (CB) oscillation characteristics observed for oxidised PC-Trs (Oxidised A and B).

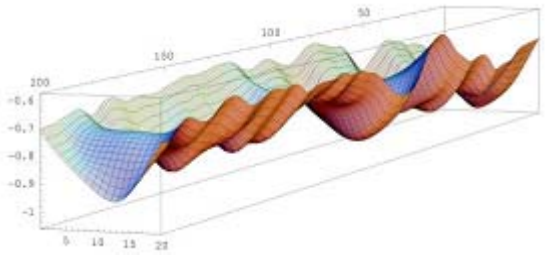

Fig. 5. Bare dopant potential landscape calculated for a NW with a mean donor concentration of 10^{19} cm^{-3}.

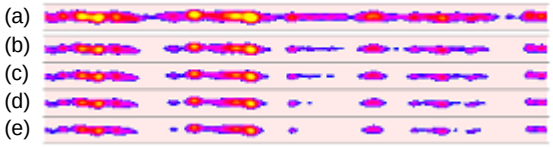

Fig. 6. Electron density distributions simulated for various Fermi energies. A mean donor concentration is 10^{20} cm^{-3}.

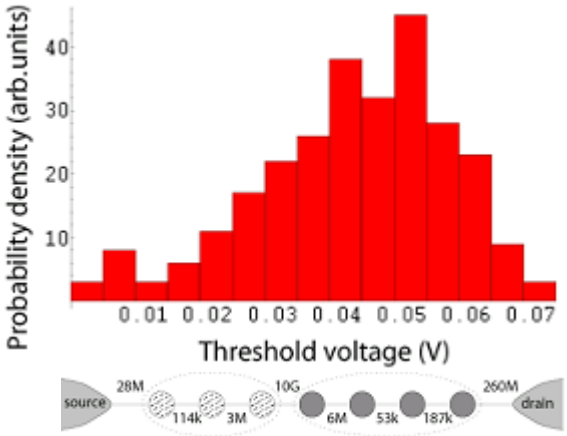

Fig. 7 Threshold voltage Vth distribution calculated for the NW structure in Fig. 6. Bottom figure shows a schematic two-macro-island system with some of the smallest tunnel resistances (in Ω) between the seven islands